Minerals Engineering 102 (2017) 42–57

Contents lists available at ScienceDirect

Minerals Engineering

journal homepage: www.elsevier.com/locate/mineng

Characterization of potassium agrominerals: Correlations between petrographic features, comminution and leaching of ultrapotassic syenites

Davide Ciceri, Marcelo de Oliveira, Rebecca M. Stokes, Taisiya Skorina, Antoine Allanore *

Department of Materials Science and Engineering, Massachusetts Institute of Technology, 77 Massachusetts Avenue, Cambridge, MA 02139, USA

ARTICLE INFO

Article history:
Received 14 November 2016
Revised 29 November 2016
Accepted 29 November 2016

Keywords:
Agrominerals
Comminution
Fertilizers
K-feldspar
Leaching
Potash

ABSTRACT

Growth of world population and consequent growth of food demand are drivers of expansion and intensification of agriculture. High-yield agriculture relies on fertilizers that, therefore, become a key focus to address concerns on global food security. Currently, potassium fertilizers are produced in the northern hemisphere. These fertilizers do not suit the deep leached soils of tropical countries, partly due to their high solubility. The use of geological materials (agrominerals) such as K-bearing silicates could be an option to develop slow release potassium fertilizers from abundant and readily available geologic sources. Thus far, both laboratory and agronomic field tests on such materials have been inconclusive, meaning that a clear relationship between the application of agrominerals to soil and the fertilizing effect could not be established. Novel interdisciplinary approaches are needed to predict the release of nutrients from agrominerals. This study presents one such approach, proposing a detailed analysis of the relationship between petrographic characteristics of twelve samples of ultrapotassic syenite (K-feldspar ore), and the leaching of potassium from their powders. The correlation between petrographic features, comminution and leaching proposed here, is expected to play a major role in the assessment of the fertilizing properties of agrominerals in the field.

© 2016 Elsevier Ltd. All rights reserved.

1. Introduction

Feeding the world in sustainable ways is a major challenge that humanity will have to face in this century (Tilman et al., 2011; Foley and et al., 2011; Pretty and et al., 2010; Tollefson, 2010; Baligar et al., 2001). Increasing population - models forecast a total number of about 9 billion people by the year 2050 (Pretty and et al., 2010; World Population Prospects, 2012) - and decreasing accessibility to agricultural lands, are questioning the current status of global food security (Tilman et al., 2011; Pretty and et al., 2010; Baligar et al., 2001; Manning, 2010; Van Straaten, 2006). Innovation and a conjunct multidisciplinary effort are necessary to tackle dietary changes, food distribution and waste, as well as an increase of agricultural yields in less productive soils. Fertilizers are key enablers of both expansion and intensification of agriculture, since they replenish the nutrients (primary: N, P, K; or secondary: Mg, Ca, S, Na, B, Mn, Fe, Ni, Cu, Zn, Mo), that are removed from soils by both harvesting, naturally occurring and pervasive leaching.

This work focuses on potassium fertilizers, referred to as *potash* when traded on international markets (Ciceri et al., 2015). Currently, some countries in the Global South are unable to locally produce the amount of potash necessary to expand and/or intensify their agriculture, or simply maintain an adequate K balance in their soils (Ciceri et al., 2015; Teng et al., 2001; Leonardos et al., 2000; Skorina and Allanore, 2015). For example, both India and Brazil need to import >90% of the potash required for farming (Tollefson, 2010; FAOSTAT database; Jena and et al., 2014). Further to the economic burden paid by either governments or farmers, there are concerns that, when available, commercial potassium fertilizers might be inefficient or inappropriate to improve crop yields (Baligar et al., 2001; Manning, 2010; Van Straaten, 2006; Leonardos et al., 2000; Han et al., 2006; Khan et al., 2014). Therefore, although a renewed interest in techniques that reduce the amount of fertilizers is observed (Trewavas, 2001; Rigby and Cáceres, 2001), tropical agriculture calls for the formulation of a new generation of fertilizers. Those have to be locally available - to reduce cost and facilitate transport within countries with limited infrastructure -, and provide the nutrients at a rate that matches the needs of crops

* Corresponding author.
E-mail addresses: ciceri@mit.edu (D. Ciceri), marceloo@mit.edu (M. de Oliveira), m.rebecca.stokes@gmail.com (R.M. Stokes), tskorina@mit.edu (T. Skorina), allanore@mit.edu (A. Allanore).

http://dx.doi.org/10.1016/j.mineng.2016.11.016
0892-6875/© 2016 Elsevier Ltd. All rights reserved.

in tropical soils. In this context, nutrient-rich geological materials (agrominerals) have been discussed as an alternative to commercial soluble potash (Leonardos et al., 2000). Distinct advantages of *agrominerals* are (i) global widespread availability, (ii) simple processing generally involving only comminution (crushing, grinding and sieving), and (iii) continuous delivering of nutrients to soil over several agronomic cycles (Manning, 2010; Van Straaten, 2006, 2002; Leonardos et al., 2000; Skorina and Allanore, 2015; Harley and Gilkes, 2000). However, a key concern for these resources is the leaching rate of macronutrients, often considered too low (10^{-11} to 10^{-13} mol_{K+} m^{-2} s^{-1} in the acidic pH range (Manning, 2010; Skorina and Allanore, 2015; Blum, 1994)) in comparison with conventional salts. Weathering transforms primary minerals into secondary minerals, and is partly responsible for the rate of nutrient leaching into the soil solution from agrominerals. A vast literature on weathering reactions discusses the properties of ground minerals contacted with leaching solutions (Blum, 1994; Wilson, 2004; Hellmann and et al., 2012; Hartmann and et al., 2013; Berner and Berner, 1997; Lasaga and Luttge, 2001; White and Brantley, 1995), and the interest of agronomists for agrominerals leads to a resurgence in the use of the "pot test". In this latter configuration, the reactivity of minerals comminuted and subsequently mixed with soil is assessed in the presence of growing crops (bioweathering) Manning, 2010; Van Straaten, 2006, 2002; Leonardos et al., 2000; Han et al., 2006; Harley and Gilkes, 2000; Coroneos et al., 1996; Wang et al., 2000; Abdel-Mouty and El-Greadly, 2008; Weerasuriya et al., 1993; Von Wilpert and Lukes, 2003; Hinsinger et al., 1996; Somerwill and et al., 2012; Bakken et al., 1997.

At industrial scale, comminution of geological materials occurs in equipment such as jaw crushers, for 10^1 millimeter-sized crushing (Bakken et al., 1997, 2000), and either ball mills (Bakken et al., 1997, 2000; Sánchez et al., 2004) or High-Pressure Grinding Rolls (HPGR) Schönert, 1988; Tavares, 2005 for 10^{-1} millimeter-sized fine-scale grinding. Particle Size Distribution (PSD) and Specific Surface Area (SSA) are key parameters used to describe comminuted ores (Table 1). Generally, SSA is measured either in a geometric way (G-SSA) or with the Brunauer, Emmet and Teller method (BET-SSA). Despite the *physical* meaning of SSA being immediate and intuitive, its *chemical* meaning is not. The area effectively available for nutrient leaching, i.e. the *reactive surface area*, differs from both G-SSA and BET-SSA (White and Brantley, 1995). As an example, Holdren and Speyer (Holdren and Speyer, 1985, 1987) demonstrated the existence of three different size-dependent leaching rates for feldspar, which were explained by the density of defects and by non-linear changes in SSA during leaching. Comminution determines the type and density of surface defects (mechano activation) (Jena and et al., 2014; Sánchez et al., 2004; Vogel and Peukert, 2003) and therefore the reactive surface area of any agromineral. Sánchez et al. (2004) used a planetary ball mill on anorthoclase to demonstrate increased agglomeration of fine particles and amorphization with increasing grinding time. Priyono and Gilkes (2008) demonstrated clear improvements in agronomic yields when over-milled feldspathic gneiss (1 h ball mill) was added to soils. However, for large-scale operations such as those required by the fertilizer industry, the cost efficiency of mechano activation remains unclear (Priyono and Gilkes, 2008, 2004; Kleiv and Thornhill, 2007). Detailing the type of milling and assessing parameters such as SSA and PSD remains nevertheless of critical importance to standardize results obtained from agronomic weathering experiments.

K-feldspar ($KAlSi_3O_8$) is the most abundant K-bearing agromineral. Typically, it occurs both in granites (*lato sensu*) in a relatively low concentration (~25 wt% corresponding to ~4.2 wt% K_2O) and in ultrapotassic syenites in a high concentration (~85 wt% corresponding to ~14.3 wt% K_2O). The relatively high potassium content and the availability on the Earth surface of high-purity K-feldspar rocks such as ultrapotassic syenites make comminuted K-feldspar a material worth considering as an alternative potash fertilizer (Manning, 2010). However, attempts in this direction have been unsuccessful thus far, presumably due to the slow leaching rate of framework potassium from K-feldspar (Manning, 2010; Priyono and Gilkes, 2008; Gautneb and Bakken, 1995; Mohammed et al., 2014). Here, it is important to point out that a single label "K-feldspar" is often inadequate to describe the raw material, since a range of elemental compositions, polymorphic structures and petrographic characteristics are possible. An additional critical aspect is the crystallization history, which will likely affect the potassium-leaching rate from the feldspar to the soil. The higher the Al-Si ordering, the higher the stability of structural K^+ located in the interstitial sites of the K-feldspar, and the lower the leaching rate. Al-Si ordering might also be key for the response of bulk agrominerals to comminution. As demonstrated in the present work, such a broad range of properties can be observed in syenite. Therefore, while on geological timescales different syenite rocks follow approximately the same chain of weathering reactions, on agronomic timescales other important parameters are overlooked. Those include the variety of K-feldspar, the accessory phases (e.g., titanite, apatite, pyroxenes, micas, and amphiboles), and the physical-mechanical properties such as twinning, lamellae

Table 1
Overview of parameters relevant in the characterization of comminuted ores.

Variable	Description	Technique	Value for K-feldspar	Ref
Geometric Specific Surface Area (G-SSA)	Total surface available per mass unit calculated according to geometric considerations (does not take into account surface roughness and porosity)	Laser diffraction of a suspension of powder samples; image analysis of photographs of mounted samples	0.005–0.060 m^2 g^{-1}	Blum (1994), White and Brantley (1995), Merkus (2008), Allen (1997)
Brunauer, Emmet and Teller Specific Surface Area (BET-SSA)	Total surface available per mass unit as measured from gas adsorption. Take into account surface roughness and porosity (micropores <2 nm; mesopores 2–50 nm; macropores >50 nm)	Isothermal adsorption of gas molecules, generally N_2 or Kr, at the surface of the material	0.04–1.02 m^2 g^{-1}	Blum (1994), Merkus (2008), Allen (1997), Brunauer et al. (1938)
Reactive Specific Surface Area	Surface area that takes effectively part in chemical reactions	A standard method is not available although dye adsorption and colorimetric methods have been proposed	n/a	Hang and Brindley (1970)
Particle Size Distribution (PSD)	Relative amount in percentage of the total volume (or of the percentage of the total number of particles) for any specific size of particle that constitutes a powder	Laser diffraction of an appropriate suspension of the powder sample	Varies with grinding techniques. Standard ball mills lead to smallest particles in the order of 15 μm and a distribution peak between 50 and 500 μm	Merkus (2008), Allen (1997)

or recrystallization structures, which have not been investigated thus far. A comprehensive characterization of the raw materials and their relationship to comminution have been neglected in agronomic studies, as shown by insufficient, or lack of, petrographic description, PSD and SSA determinations as well mineralogical and/or elemental analysis (Manning, 2010; Coroneos et al., 1996; Wang et al., 2000; Abdel-Mouty and El-Greadly, 2008; Weerasuriya et al., 1993; Hinsinger et al., 1996; Bakken et al., 1997, 2000; Badr, 2006; Scovino and Rowell, 1988; Bolland and Baker, 2000). Recently, a detailed study investigated feldspar mechano activation, highlighting the necessity to understand the correlation between the properties of the powders and the leaching of agricultural nutrients (Kleiv and Thornhill, 2007).

In this contribution, we discuss quantitatively the relationship between petrographic characteristics of twelve ultrapotassic syenites, and potassium leaching from their comminuted powders. We show that (i) in absence of major defectual structures created by comminution, the potassium leaching from syenite powders can be attributed mainly to specific thin section-scale petrographic features of bulk ore samples (ii) comminution can be performed effectively regardless the nature of the raw material, taking into account variation in petrographic features (iii) prolonged comminution in a ball mill (over milling) results in enhanced leaching of nutrients, which, however, becomes uncorrelated to the petrographic features visible with optical methods. The findings of the present work can be used by agronomists to develop meaningful formulations and guidelines for the application of agrominerals as alternative potash fertilizers.

2. Materials and methods

2.1. Geological considerations on syenites

We investigate a set of twelve syenites that are derived from ultrapotassic, silica-saturated magmatism (Thompson and Fowler, 1986), and commonly formed by melting of lithospheric sources that results in small magma volumes. Syenites do not evolve by fractional crystallization, and tend to occur as clusters of small intrusions, usually <10 km^2 each. Therefore, for the same syenitic intrusion in addition to metamorphic and weathering reactions, both diffusion and convection in the magma chamber can result in subtle chemical and mineralogical differences as shown by this study.

The twelve samples were obtained from the Triunfo batholith (Supplementary Fig. S1), between the municipalities of Triunfo and Serra Talhada, Pernambuco State, Brazil (38′12″W, 7′55″S) (Ciceri and Allanore, 2015; Ferreira and Sial, 1986). Overall, the Triunfo batholith is composed by at least five syenitic intrusions, consisting mainly of alkali-feldspar clinopyroxene syenites. These intrusions are located in the transversal zone of the Borborema tectonic province in Northeastern Brazil, and is characterized by granitic magmatism associated with the Neoproterozoic Brazilian orogeny (800,500 Ma). Both geochemical and mineralogical data (Sections 3.1 and 3.2) indicated that the syenitic intrusions were all generated by low degree of melting of a similar and metasomatized mantle source. Likely, all intrusions are cogenetic, but not comagmatic. Local cataclastic transformations are also present, mainly progressive fracturing of existing rocks associated with fault zones. The soils surrounding the field site are Oxic Haplustept, Typic Haplustept and Typic Haplustult. The region is part of the Caatinga biome. The rainy period is limited to ~4 months.

The samples investigated were obtained from three of the five Triunfo batholith syenitic intrusions, and were labelled as (i) ARD05, ARD21, ARD22; (ii) EBT09, EBT10, EBT12, EBT13; and (iii) MCA04, MCA11, MCA12, MCA23, MCA41. The first three letters indicate one of the three intrusions (Supplementary Fig. S1).

2.2. Comminution and characterization of syenites

2.2.1. Petrographic thin sections

Petrographic thin sections were obtained from all twelve syenite samples (Spectrum Petrographics Inc.). They were 27 mm × 46 mm, 30 μm thick, two-sided polish (0.5 μm diamond) and mounted on borosilicate glass with acrylic resin. A petrographic microscope (Olympus BX51) was used to observe the thin sections, identify minerals, and describe magmatic, late-magmatic and post-magmatic textures (Section 3.1) (Smith and Brown, 1988). Digital photographs of thin sections were instead analyzed with a combination of Adobe Photoshop CC 2014® and ImageJ (ImageJ). For each thin-section sample, number-averaged (d_i) and area-averaged (d_A) grain sizes were determined, as well as the average Aspect Ratio ($\overline{AR}$) of the grains. A detailed protocol is given in Supplementary Text S1.

2.2.2. Comminution

Powders for all twelve syenite samples were obtained according to three distinct procedures, generating four sets of powders (Supplementary Text S2). In order to obtain powders with similar size distributions, and relevant to industrial settings, the operator used a different milling time and energy for each of the syenites (Supplementary Table S2).

The first procedure used a jaw crusher to reduce ~25 kg of each field sample into pieces <4.75 mm. Approximately 15 kg of this finer material were comminuted in a roller crusher to obtain a fraction <1.00 mm. Next, 1.7 kg of this latter fraction were screened for particles <150 μm; particles that did not respect such a criterion (i.e., particles >150 μm) were ball milled (Furlan 6595C, 600 cm^3) with stainless steel balls, with an iterative procedure (Supplementary Fig. S4a). For each syenite, the fractions <150 μm were collected together and labelled as *Standard Samples* (SS).

The second procedure used a slightly different workflow. Specifically, 2.2 kg of the fraction <1 mm from the roller crusher were continuously comminuted in the ball mill until all the material passed through a sieve of 150 μm. Samples obtained from this procedure were labelled as *150 Over Milled* (150OM). For a second subset the procedure was the same, other than the fact that the fraction <1 mm from the roller crusher was continuously comminuted in the ball mill until all the material passed through a sieve of 45 μm. Samples obtained from this procedure were labelled as *45 Over Milled* (45OM) (Supplementary Fig. S4b).

The third procedure used between 7.5 kg and 11.5 kg of the fraction <1.00 mm from the roller crusher for comminution in a HPGR 30 cm × 60 cm (METSO, HRC300). The powder obtained from the HPGR was screened for particles <150 μm; particles >150 μm were comminuted again in the HPGR with an iterative procedure. For each of the syenite samples, fractions <150 μm were collected together and labelled as *HPGR samples*.

2.2.3. X-ray Fluorescence (XRF)

The elemental content of the syenites was determined by X-ray Fluorescence (XRF). The analysis (SGS Geosol Laboratórios Ltda.) was handled according to certified quality management system ABNT NBR ISO 9001:2008. Before analysis, rock samples were dried, manually crushed to 2 mm, quartered and milled with a steel ball until 95% of the material passed through a 150 μm sieve. Subsequently, the method of fusion in presence of lithium tetraborate was used. The powders used for XRF analysis were considered as the best proxy of the powders obtained from comminution procedures.

2.2.4. X-ray powder diffraction (XRPD)

The mineralogical content of the syenites was determined by X-ray Powder Diffraction (XRPD). Before analysis, 3 g of the 2 mm

rock fraction (obtained by sieving the material from the jaw crusher described in Section 2.2.2) were micronized in wet (aqueous) conditions for 5 min (Glen Creston, McCrone micronizing mill). Stacked bits of corundum were used as the micronizing media. Although this procedure might introduce unwanted strains in the syenite samples, such an effect is assumed to be negligible. The micronized powders were considered as the best proxy of the powders obtained from comminution procedures. XRPD analyses were carried out on a PANalytical X'Pert Pro Diffractometer with a Cu X-ray source. Data collection conditions were optimized for quantitative Rietveld refinement. Scans were run from 5 to 70° 2θ using a 0.0167° step-size and a scan speed of 200 s per step. A Soller slit size of 0.02 radians was used in addition to a 10 mm beam mask and 2° incident beam antiscatter slit. A Ni filter was used to filter Cu Kβ radiation. Rietveld refinement of the Xray diffraction patterns was performed using PANalytical's – HighScore Plus software. Crystallite size analysis was preformed using LaB6 NIST 660a standard for the contribution of instrument broadening.

2.2.5. Particle size distribution (PSD) and geometric surface area (G-SSA)

The particle size distribution of all powders (Standard Samples, 150OM, 45OM and HPGR) was obtained with a laser diffraction particle size analyzer, equipped with an aqueous liquid module (Beckman Coulter Inc., LS 13 320). The principle of the analysis is discussed elsewhere (Allen, 1997; Hodson, 2006). Samples were sonicated at 20 kHz and 18 W for 1 min before analysis. The software permitted to estimate the G-SSA for each of the samples. Garnet.rf780z was chosen as the optical model. Density was assumed to be 2.6 g cm^{-3} for all samples. The smallest particle size detectable with the technique is 0.017 μm.

2.2.6. Brunauer, Emmet and Teller surface area (BET-SSA)

Surface area measurements of all powders (Standard Samples, 150OM, 45OM and HPGR) were performed with a Micromeritics® ASAP 2020 surface area and porosity analyzer. The samples (about 0.3–0.5 g of each powder) were degassed at 200 °C for 12 h, or until a constant vacuum level of 10^{-5} mmHg min^{-1} was reached in the sample tube. The final value of BET-SSA was determined on the adsorption branch with the multi-points method, in the p/p_0 range of 0.08–0.24. Krypton was the gas used for adsorption. An independent test on a selected sample (MCA12) demonstrated that the reproducibility of SSA determination was within a variation of 2.5%. The accuracy was >95%, as determined with SSA standards (Micromeritics® silica-alumina 214 ± 6 m^2 g^{-1} and Micromeritics® alumina 0.25 ± 0.03 m^2 g^{-1}).

2.2.7. Mounting of powders for scanning electron Microscopy (SEM)

For imaging purposes, powders (Standard Samples, 150OM, 45OM and HPGR) were mounted in epoxy using castable molds. After hardening, the powder mounts were polished with a rotative system. Mounted powders were gold coated and imaged with a scanning electron microscope (JEOL 6610 LV) in either high-vacuum (<10^{-3} Pa) or low vacuum (90 Pa) mode. The accelerating voltage was 15 kV, the spot size was set to 50–60, the working distance set at 14–17 mm. All images were obtained by using the backscattering detector at a magnification of ×270.

2.2.8. Leaching tests

The elemental leaching from all powders was assessed with conventional batch tests. Approximately 1 g of syenite powder was suspended in 10 mL of a standardized solution of HNO_3 0.1 M (Alfa Aesar), in a plastics test tube. The test tube was rotated continuously for 24 h. The solution was centrifuged for 5 min and the clear supernatant was filtered through a syringe filter 0.45 μm (Whatman 13 mm GD/X). Centrifugation and filtering were both carried out within 15 min of stopping the rotator. For a few selected samples, the pH after leaching was checked with a pH paper, and shown to remain constant at pH = 1. Each leaching test was repeated three times. The concentration of K, Al, Si, Na, Ca, Mg, and Fe in the filtered solution was determined by Inductively Coupled Plasma Mass Spectroscopy (ICPMS, Agilent Technologies 7700 Series). The instrument used an Octopole Reaction System (ORS) that was run in "He mode" (He = 4.0 mL min^{-1}) except for Ca, which was determined in "no-gas mode". The ICP-MS calibration curve was obtained by an appropriate dilution of elemental standards at 1000 ppm (TraceCERT®, Fluka Analytical) in standardized 0.1 M HNO_3 (Alfa Aesar). Three wash cycles at increasing concentration of HNO_3 (0.01 M, 0.1 M and 0.5 M) were performed between the analysis of each sample. An acidic solution (pH = 1 from HNO_3) of In at 1 ppm was used as the internal standard.

The extraction efficiency was obtained according to Eq. (1):

$$\xi = \left(\frac{1}{SA}\frac{K_2O_{(sol)}}{K_2O_{(bulk)}}\right) \times 100 \quad (1)$$

where ξ (% m^{-2}) is the extraction efficiency per surface area unit, $K_2O_{(sol)}$ is the amount of K_2O (g) determined in the leaching solution after 24 h (this is measured with ICP-MS), $K_2O_{(bulk)}$ (g) is the total amount of K_2O in the powder sample being leached (this is calculated by considering the actual mass of the sample leached and the K_2O content of the sample determined by XRF), and SA is the surface area (m^2) of the sample (this is calculated by considering the actual mass of the sample leached and the BET-SSA). The same considerations were applied to each of the element analyzed. Normalizing by BET-SSA was deemed necessary to provide a meaningful comparison across the twelve syenites, which exhibited a relatively large variation in surface areas, as shown later in Fig. 5b. However, the following considerations need to be stressed (i) BET-SSA does not necessarily represents the reactive surface area, (ii) non-linear changes of BET-SSA can occur during leaching and (iii) not all elements are homogeneously distributed at the surface. Further details are discussed later, in Section 3.2.5.

For each leaching test, the experimental uncertainty, σ, associated with the extraction efficiency was determined by error propagation theory (Skoog et al., 2013), assuming: (i) 10% error on concentration determined by ICP-MS, (ii) 10% error on XRF values, and (iii) 10% error on the surface area, to account for possible changes in SSA during leaching. Error on the mass of the weighted sample was neglected. The total uncertainty σ_{tot} plotted as an error bar was determined according to Eq. (2), considering that the final extraction efficiency ξ is obtained as the average of three replicates:

$$\sigma_{tot} = \sqrt{0.03} \times \sqrt{(\xi)^2_{rep1} + (\xi)^2_{rep2} + (\xi)^2_{rep3}} \quad (2)$$

where ξ for each of the replicates is given by Eq. (1).

2.2.9. Principal component analysis (PCA)

Selected experimental data were subjected to a Principal Component Analysis (PCA) with standardized scores (Jolliffe, 2002). PCA was performed with Origin (OriginLab, Northampton, MA). Only two components were extracted, accounting for as little as 54.7% of the total variance for Standard Samples and as much as 81.5% of the total variance for HPGR samples. Due to both the relatively small variance and number of observations, PCA results can be regarded exclusively as an estimation, but they still provide a good path to pattern recognition in the syenites behavior.

3. Experimental results

3.1. Petrographic description of thinsection samples

Petrography examines and evaluates the optical properties and microstructural characteristics of thin-section samples of a given

ore (Smith and Brown, 1988). For minimum cost, thin sections provide information on mineral (i) phases (ii) grain sizes and texture (iii) degree of deformation and (iv) alteration. Grains of different mineral polymorphs such as microcline and orthoclase can be distinguished in thin section despite their identical chemical composition of $KAlSi_3O_8$ (Smith and Brown, 1988). An overview of syenite photomicrographs is given in Fig. 1. K-feldspar and pyroxene minerals were clearly distinguishable from each other (Fig. 1a). Tartan twinning such as those observed in Fig. 1(a), (b) and (i), are a distinct feature of microcline crystals rather than orthoclase, which can often show Carlsbad twinning (Smith and Brown, 1988). For some samples, perthitic exsolution lamellae were visible (Fig. 1 (a) and (b)). A detailed petrographic description revealed that in all of the three intrusions investigated (ARD, EBT and MCA), rocks are equigranular clinopyroxenealkali-feldspar syenites, with original igneous textures well preserved (Table 2). Specificities for each intrusion are as follow:

Rocks from the ARD intrusion display equigranular, medium (ARD22) and medium-to-coarse (ARD05 and ARD21) grained textures, and are slightly fractured (Fig. 1c). ARD05 is the sample with best preserved K-feldspar, only slightly altered (sericitization) and fractured. Crystals are subhedral to euhedral, with well-developed perthite textures. K-feldspar crystals are subhedral to anhedral in both ARD21 and ARD22. However, they are smaller, more altered and more fractured in ARD22 than in ARD21.

Rocks from the EBT intrusion display equigranular, medium-to-fine (EBT09 and EBT10), medium (EBT13) and medium-to-coarse (EBT12) grained textures. They contain clinopyroxene, most likely aegirine, as their principal mafic mineral, and titanite ± apatite as primary accessory minerals. EBT10 shows subhedral medium and fine K-feldspar crystals, with moderate to abundant alteration features; the deformation has a brittle character, with moderate fracturing of the whole rock. EBT09 shows fractured anhedral K-feldspar crystals, with strong sericitization. EBT12 shows

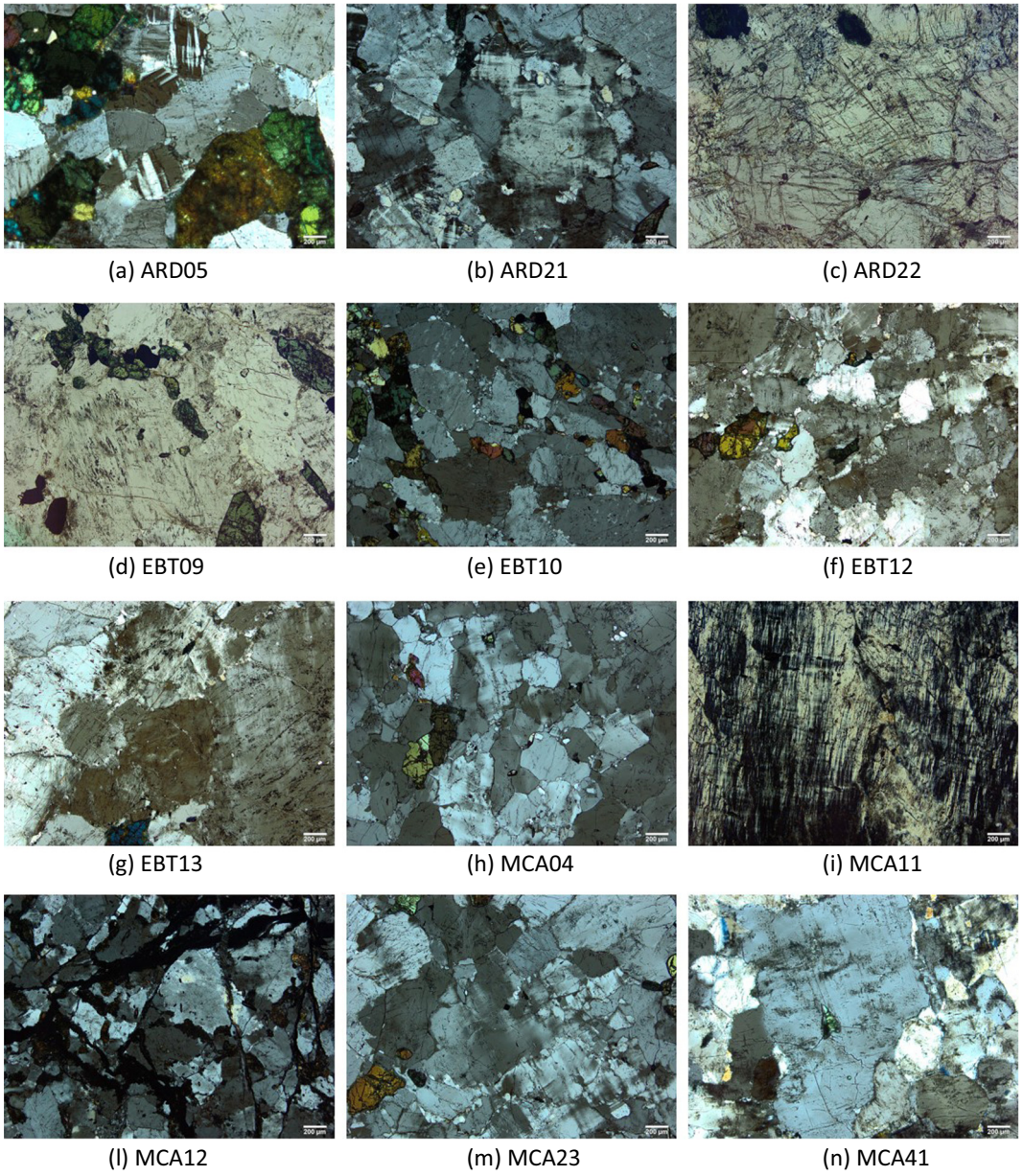

Fig. 1. Overview of photomicrographs of the twelve syenite samples in thin section. (c) ARD22 and (d) EBT09 are in parallel polarized light whereas all other samples are in cross-polarized light. 200 μm scale bar applies to all micrographs.

Table 2
Overview of petrographic characteristics of syenite samples.[a,b] Samples are listed according to the leaching forecast within each intrusion.

Sample	Kfs texture	Kfs shape	Kfs texture[c]	Alteration	Recrystallization	Fracturing	Mafic minerals	Opaque minerals	Modal contents	Ranking
ARD22	Medium (M)	Subhedral to anhedral	Microperthite	Medium to low	Medium	Medium, in the Kfs crystals	Cpx, Amp and Bt (rare)	Mt; Mrt	86% Kfs; 12% Cpx; 1% Tit; <1% Mt; Ap, Amp and Bt (Tr)	6
ARD21	Medium to coarse (M)	Subhedral to anhedral	Cryptoperthite	Low	Low	Low	Cpx	Mt; Mrt	80% Kfs; 14% Cpx; 3% Qz; 1% Tit; 1% Ap; 1% Ox	7
ARD05	Coarse to medium (C)	Subhedral to euhedral	Microperthite	Low	No	Low	Cpx and Amp (rare)	Mt (rare)	85% Kfs; 9% Cpx; 2% Amp; 2% Tit; 1% Ap; <1% Ox	10
EBT10	Fine to medium (F)	Subhedral	Cryptoperthite	High to medium	Medium, filling the fractures and between crystals	Medium, in the whole rock	Cpx	Mt	92% Kfs; 7% Cpx; Tit 1%; Trace Ap, Mt, Amp and Ept	2
EBT09	Medium, with fine neoformed crystals (M)	Anhedral	Cryptoperthite	High	Medium, filling the fractures and between crystals	High, in the Kfs crystals	Cpx	Mt; Mrt	94% Kfs; 4% Cpx; 0.7% Tit; 0.3% Ap; 1% Ox	3
EBT13	Medium (M)	Anhedral	Cryptoperthite	High	Low	Medium, in the whole rock	Cpx and Amp (rare)	Absent	91% Kfs; 8% Cpx; 0.5% Amp; 0.5% Tit+Ap+Ox. Ept	5
EBT12	Medium to coarse (M)	Subhedral to euhedral	Microperthite	Medium	No	Low	Cpx	Absent	90% Kfs; 8% Cpx; 0.5% Tit; 0.5% Qz; Trace Ap and Amp	8
MCA41[d]	Medium, with fine neoformed crystals (M)	Anhedral	Cryptoperthite	High	Low, filling the fractures and between crystals	High, in the Kfs crystals	Cpx and Amp (rare)	Absent	92% Kfs; 6% Cpx; 1% Amp; 1% Tit; Trace Ap and Ox	1
MCA04	Medium to fine (M)	Anhedral	Cryptoperthite	High	Low	Medium to high	Cpx and Amp (rare)	Mt (rare)	90% Kfs; 9% Cpx; 0.5% Tit; 0.5% Apt	4
MCA12	Fine to medium (breccia) (F)	Subhedral to euhedral	No	No	High, filling the fractures and between crystals	Medium, in the whole rock	Cpx	Absent	Breccia	9
MCA11	Coarse to medium (C)	Subhedral to euhedral	Microperthite	Medium	Low, filling the fractures and between crystals	Low	Cpx and Bt (rare)	Absent	94% Kfs; 4% Cpx; 0.5% Bt; 1% Tit; 0.5% Ap	11
MCA23	Medium to coarse (M)	Subhedral	Microperthite	Low	Low	Low	Cpx and Amp	Absent	80% Kfs; 17% Cpx; 2% Amp; 1%Tit; Apt	12

[a] Kfs = K-feldspar, Cpx = clinopyroxene, Mt = magnetite, Mrt = martite, Bt = biotite, Ox = oxides, Ap = apatite, Tit = titanite, Amp = Amphibole, Ept = epidote.
[b] All samples are equigranular.
[c] Microperthite: Na and K-feldspar crystals can be detected with optical microscope; cryptoperthite: Na and K crystals can be detected only by X-ray diffraction or electron microprobe. See also Flude et al. (2012).
[d] MCA41 is the same sample investigated by Ciceri and Allanore with a microfluidic setup (Ciceri and Allanore, 2015).

well-preserved subhedral-to-euhedral K-feldspar crystals. Perthites are observed in all EBT samples, and are more developed in EBT12. EBT13 shows a strongly altered K-feldspar, with anhedral crystals.

Rocks from the MCA intrusion display equigranular, fine (MCA12), medium-to-fine (MCA41) and medium-to-coarse (MCA11) grained textures. MCA41 shows anhedral, medium and fine K-feldspar crystals, which are strongly altered and fractured. MCA11 shows subhedral-to-euhedral, medium and coarse K-feldspar crystals, which are well preserved, and with more developed perthites. MCA12 shows a characteristic deformational breccia, pervasive fracturing in two principal directions and strong recrystallization.

Physical and chemical properties of mineral phases define the extent of mineral alterations (Kawano and Tomita, 1995). Therefore, it can be presumed that the petrographic characteristics of the syenites (Table 2), and consequently the crystallization and subsequent alteration that can be inferred by such characteristics, can be correlated to their ability to leach potassium and other agricultural nutrients. Key petrographic considerations with respect to the expected leaching behavior are as follow:

The Al-Si ordering of K-feldspar in igneous rocks is related to petrologic conditions such as temperature, pressure and bulk composition. For a given mineral phase, rate of both nucleation and crystal growth depends on the magma cooling rate, which may be inferred by the size and shape of K-feldspar crystals (Swanson, 1977). Moderate-to-high cooling rates result in medium to fine grains, with subhedral to anhedral shapes and low AlSi ordering in the feldspar. Presumably, the framework K^+ from such feldspar will be more mobile, and leach at the faster rate when the syenite surface will be contacted with the soil solution at agronomic time scales. Conversely, a low cooling rate results in medium-to-coarse grains, with subhedral to euhedral shapes and feldspar with high Al-Si ordering, which would result in a slower potassium leaching.

Development of perthitic textures in K-feldspar is dependent on both cooling rate and range of crystallization temperature (Brown and Parsons, 1984). The higher the cooling rate the smaller the development of perthites (microperthite), and the lower the Al-Si ordering in the feldspar. Again, this would lead to an enhanced K^+ leaching upon contacting the syenite surface with leaching solutions.

Late and post magmatic processes are an additional key factor, which can be inferred from petrographic thin sections. Features such as fracturing and pre-existing mineral alterations (sericitization or argilitization) suggest samples that have undergone physicochemical processes (e.g., hydrothermal), which might decrease structural ordering, and hence favor K^+ leaching. In these cases, fractures and alteration features at a length scale that is smaller than that of powder particle might act as channels that facilitate the percolation of leaching solution into the bulk structure, and therefore enhance surface area and the release of K^+.

A holistic understanding of the crystallization history, late to post magmatic alterations and leaching behavior, is better achieved through petrography and its descriptors rather than X-Ray Fluorescence (XRF) and X-Ray Powder Diffraction (XRPD) analyses (Section 3.2.1). Based on our overall reasoning, a ranking of the potassium leaching capacity in acidic conditions is proposed in the last column of Table 2. Number 1 indicates the sample is expected to leach the more; number 12 indicates the sample is expected to leach the less. Such a petrographic forecast is shown to be in good agreement with actual leaching data discussed in Section 3.2.5.

Results of imaging analysis of the digital photographs of thin sections (Section 2.2.1) is shown in Fig. 2. Both number (d_N) and area (d_A) averaged grains diameters are proposed (Supplementary Text S1). ARD05 and MCA11 exhibit markedly larger grains than the rest of the samples. Values of d_A are consistent with petrographic observations, confirming the validity of the digital photograph approach in estimating grain sizes for internal comparison of samples. However, number-averaged sizes (d_N) are a relatively poor representation of the grain size classification based on petrographic observations. The average aspect ratio $\overline{AR}$ was selected as the shape descriptor, and shown to be very similar in all samples, ranging from 1.72 for MCA04 to 1.81 for MCA11 (Supplementary Text S1). Overall, a pixel-based quantification of grain sizes and shapes provides only limited information on samples with different geological histories (i.e., from different

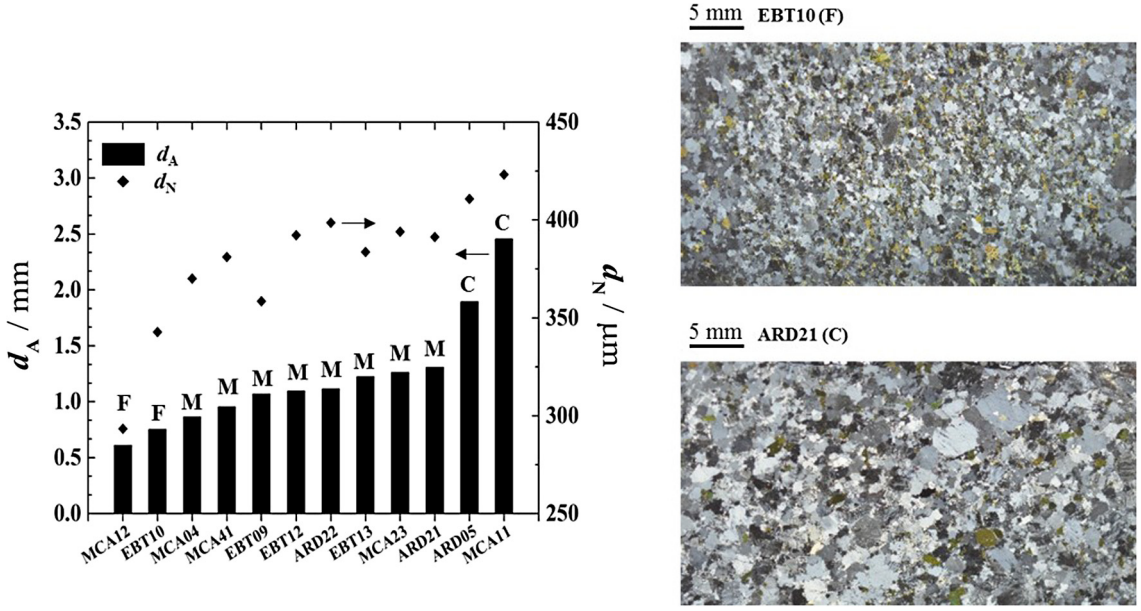

Fig. 2. Average grain diameter in thin section: d_A area averaged (reads on the left *y*-axis); d_i number averaged (reads on the right *y*-axis). Petrographic size classification according to Table 2 is shown as a bold capital letter: F for medium-to-fine and fine-to-medium samples, M for medium samples and C for medium-to-coarse and coarse samples. Digital photographs of thin sections of two selected samples are reported for visual observation and naked-eye comparison.

intrusions and with different crystallization histories). Nevertheless, this is still an efficient method for preliminary screening and classification of large libraries of geological samples, especially in settings with limited access to scientific equipment, where agrominerals might be particularly useful as an alternative fertilizer. Implications for K^+ leaching are discussed later in Section 3.2.5.

3.2. Physicochemical characterization of powder samples

3.2.1. Elemental and mineralogical composition

Based on data from Rietveld refinements of XRPD patterns, the samples analyzed in this study have mineralogies dominated by K-feldspar (typically >80 wt%) which was further delineated by the relevant K-feldspar polymorphs, orthoclase and microcline (Table 3). While both microcline and orthoclase are present in all samples, microcline is the most abundant with values ranging between 59 to 75 wt%, whereas orthoclase values range between 10 to 27 wt%. Samples also contain variable amounts of albite and pyroxene, and trace amounts of actinolite, apatite, quartz, titanite, and biotite. Albite is typically observed as small grains along grain boundaries between larger K-feldspar grains, or as perthitic intergrowths with K-feldspar (Fig. 1). Actinolite is most abundant in samples MCA11 (~3.0 wt%) and MCA12 (~8.0 wt%) and occurs exclusively associated with pyroxene, either as over growths on pyroxene rims or partial replacement of pyroxene.

One sample, MCA41, was also analyzed via XRPD to assess both the mineralogical and crystallinity changes with milling. Fig. 3 shows a small portion (20°–37° 2θ) of the XRPD patterns of the 45OM sample from MCA41, which was milled the most intensely, and the corresponding Standard Sample, which was milled the least. Qualitatively, it is clear that the 45OM sample has relatively broader peaks than the standard sample. Another notable feature is the decrease in intensity for all albite peaks, which would indicate a decrease in the total amount of albite from the Standard Sample to the 45OM sample. These qualitative observations are corroborated by Rietveld analysis, which shows that the albite concentration decreases from 16.8 wt.% in the Standard Sample to 6.8 wt% in the 45OM sample. Crystallite size analysis shows that the

Table 3
Overview of mineralogical composition from XRPD analysis (wt%) of the syenite samples. Only the main mineral phases are shown.

Sample	Microcline	Orthoclase	Albite[a]	Pyroxene	Total
ARD05	65.1	10.1	14.4	9.1	98.7
ARD21	66.0	14.9	3.5	3.5	87.9
ARD22	73.2	5.1	11.9	7.9	98.1
EBT09[b]	56.3	6.1	23.2	11.4	97.0
EBT10	68.0	11.0	13.5	6.1	98.6
EBT12	65.5	13.7	11.6	8.0	98.8
EBT13	67.8	11.7	12.7	6.6	98.8
MCA04	62.2	22.7	7.3	5.9	98.1
MCA11[c]	75.0	12.8	5.0	0.7	93.5
MCA12[d]	61.0	19.0	10.8	1.7	92.5
MCA23[e]	62.3	20.0	0.7	6.8	89.8
MCA41	67.8	26.7	1.5	3.9	99.9

[a] Albite is mostly perthitic. Therefore, the actual K-feldspar content (microcline + orthoclase) is most likely higher than reported here (cf. Table 2).
[b] Contains 2.7% of apatite.
[c] Contains 3.2% of actinolite (amphibole), which is not common in granitoids. Here, it occurs exclusively associated in pyroxene.
[d] Contains 7.6% of actinolite (amphibole), which is not common in granitoids. Here, it occurs exclusively associated in pyroxene.
[e] Contains 8.2% of quartz.

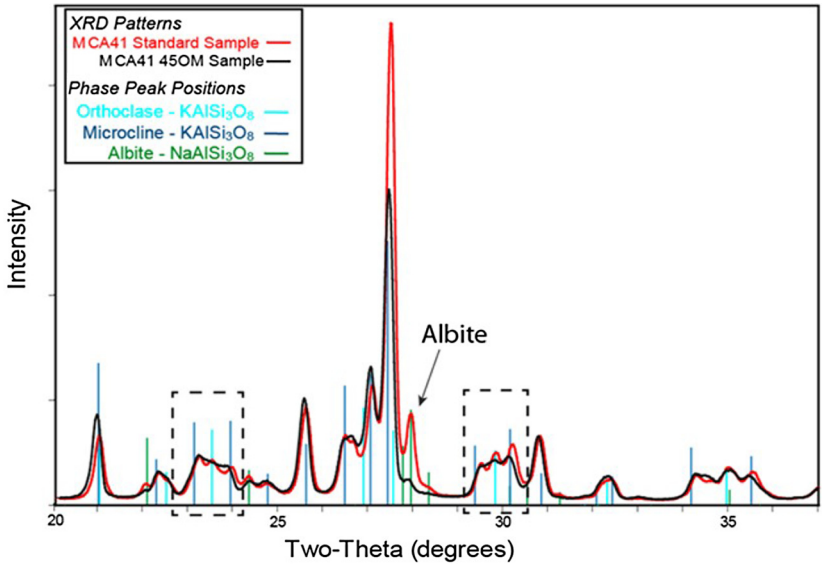

Fig. 3. X-ray diffraction patterns of MCA41 Standard Sample and MCA41 45OM shown from 20 to 37 two-theta. Also plotted are the peak positions for orthoclase (PDF: 040096197), microcline (PDF: 040081783), and albite (PDF: 040075091). The dashed boxes highlight regions of the patterns where well-defined diffraction peaks (Standard Sample) change to poorly defined diffraction peaks (45OM sample).

Table 4
Overview of elemental composition from XRF analysis (wt%) of the syenite samples.

Sample	K_2O	Na_2O	CaO	MgO	TiO_2	MnO	Fe_2O_3	P_2O_5	Al_2O_3	SiO_2	LOI	Total
ARD05	12.9	1.4	1.3	0.6	0.1	–	2.3	0.2	16.7	64.0	0.1	99.7
ARD21	13.3	1.4	1.0	0.4	0.2	–	3.0	0.1	16.8	63.5	0.1	99.7
ARD22	12.1	1.7	2.3	0.8	0.2	0.1	2.5	0.5	16.2	61.6	0.2	97.9
EBT09	13.0	1.7	1.3	0.5	0.3	0.1	2.6	0.1	17.1	62.9	0.2	99.7
EBT10	13.1	1.6	1.4	0.5	0.2	0.1	2.7	0.1	16.9	63.7	0.1	100.4
EBT12	12.1	1.6	2.5	1.0	0.4	0.1	3.9	0.2	15.5	61.7	0.1	99.0
EBT13	13.4	1.5	1.1	0.5	0.1	–	2.3	0.1	17.1	63.4	0.1	99.6
MCA04	13.6	1.1	1.3	0.5	0.2	–	2.2	0.1	16.8	62.9	0.5	99.3
MCA11	14.1	1.2	0.2	0.2	0.1	–	1.4	0.1	18.3	63.8	0.4	99.7
MCA12	12.3	1.8	2.1	0.8	0.2	0.1	3.2	0.2	17.1	62.7	0.6	101.0
MCA23	12.8	1.6	1.9	0.7	0.3	0.1	2.9	0.2	16.7	62.6	0.1	99.8
MCA41	14.3	0.7	1.3	0.7	0.2	–	2.2	0.2	17.0	62.4	0.1	99.0
Average	13.1 ± 0.7	1.4 ± 0.3	1.5 ± 0.6	0.6 ± 0.2	n/a	n/a	2.6 ± 0.6	n/a	16.9 ± 0.6	62.9 ± 0.8	n/a	n/a

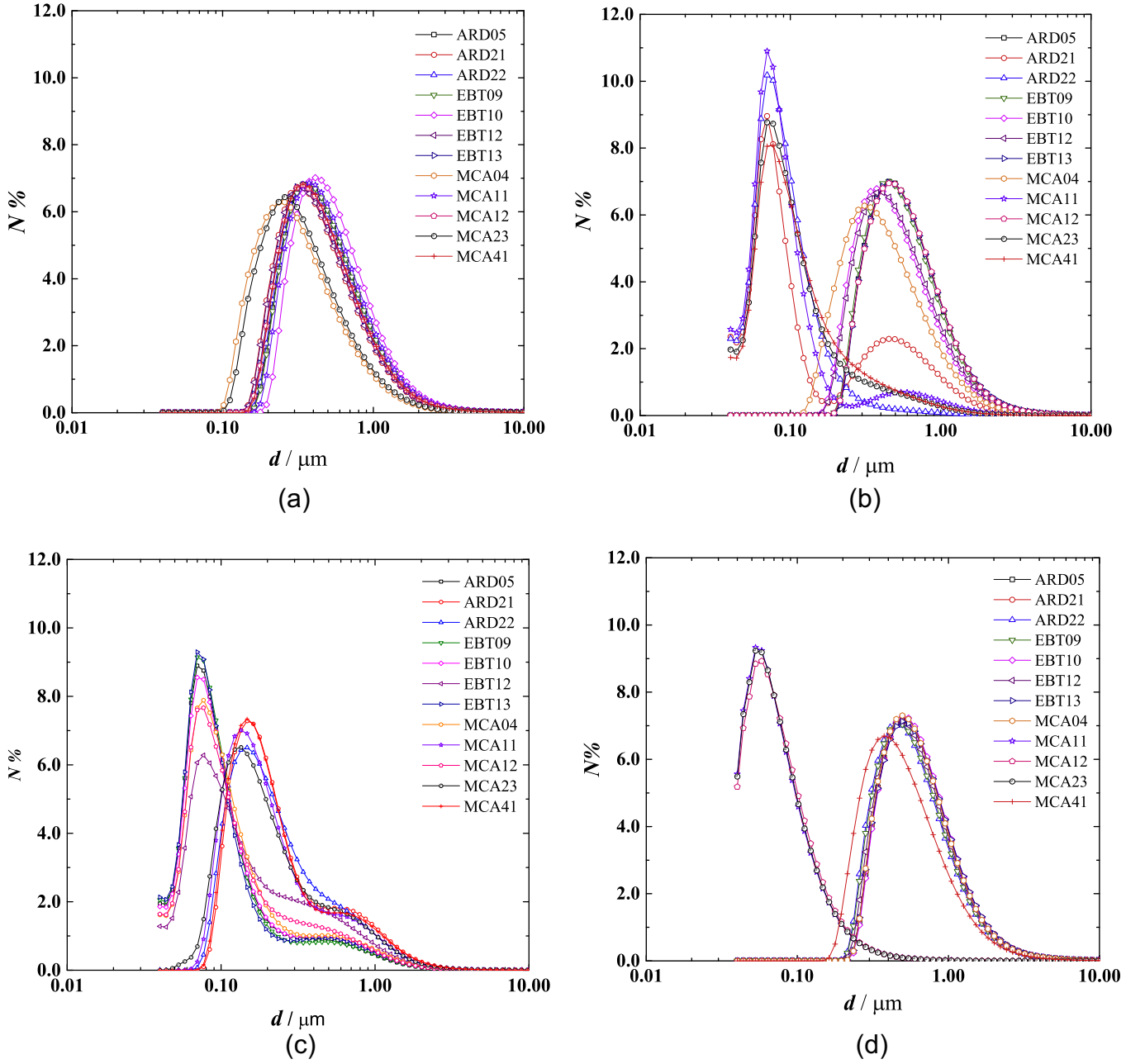

Fig. 4. Particle Size Distribution (PSD) based on the number of particles *N* for (a) Standard Samples, (b) 150OM (c) 45OM and (d) HPGR. Lower limit experimental cutoff is at 0.017 µm.

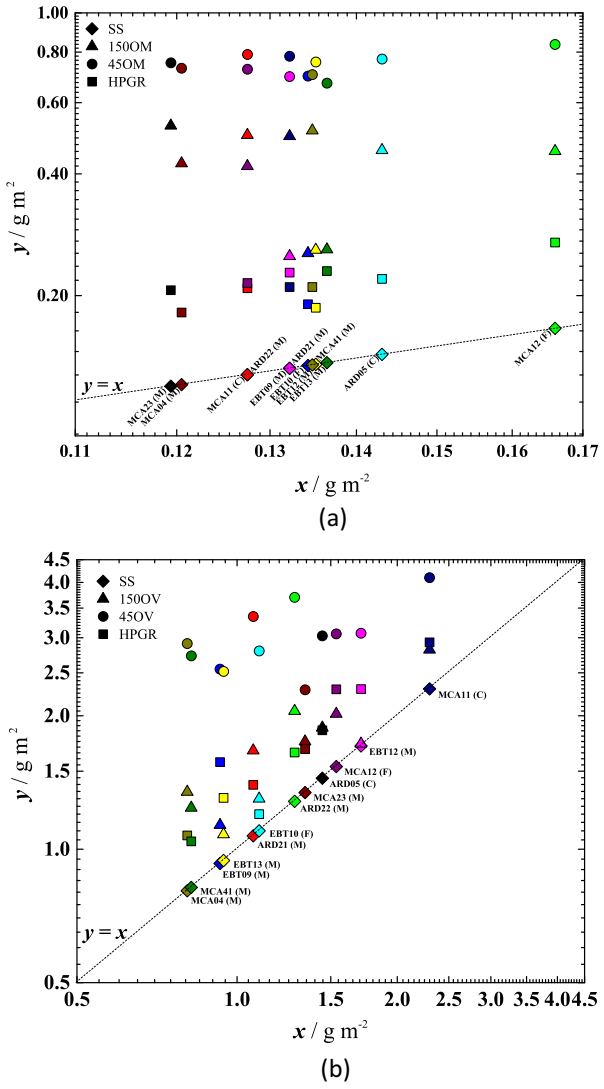

Fig. 5. Overview of syenites surface areas given as parity plot (a) G-SSA (b) BET-SSA. Samples labels are given for 150OM samples only for clarity of the graph. *x-axis* is the SSA of Standard Samples (SS); y-axis is the SSA of Standard Samples or 150OM or 45OM or HPGR. $y = x$ is given exclusively as reference. Milling time varied for each sample in order to obtain desired PSD (Supplementary Table S2). Classification of K-feldspar grain sizes in thin sections according to Table 2: F for fine-to-medium samples, M for medium, medium-to-fine and medium-to-coarse samples and C for coarse samples. In Standard Samples, G-SSA values for the couple of samples ARD22 and MCA11 as well as for the couple of samples ARD21 and EBT09 are the same.

crystallite size (or coherent X-ray scattering domain) for orthoclase decreases from 1154 ± 84 Å in the Standard Sample to 202 ± 17 Å in the 45OM sample, which causes the relative peak shape differences between samples. This is most evident in Fig. 3 where a dashed box highlights sections of the patterns where the peaks change from well defined in the Standard Sample to poorly defined in the 45OM sample.

Chemistry data obtained via XRF (Table 4) analysis corroborates the XRPD data presented here, with the exception of the low concentrations elements (<4.0 wt%) where some scatter exists between calculated chemistry from end member mineralogy and XRF chemistry. These small discrepancies can contribute to the wide variations in chemistry for a single structure (i.e., solid solution) that are not accounted for by X-ray diffraction. The chemistry for all samples is nominally similar, with SiO_2 as the most abundant species, followed by Al_2O_3 and K_2O. The rocks studied here are unusually enriched in K_2O (~13.0 avg. wt%) which reflects the high concentrations of K-feldspar in ultrapotassic syenites. Other notable elemental species include total Fe_2O_3 and Na_2O where Fe is associated with pyroxene and some magnetite (identified in thin section) and Na is associated with both albite and pyroxene.

3.2.2. Particle size distribution (PSD)

The Particle Size Distribution (PSD) in the Standard Samples, 150OM, 45OM and HPRG samples is given in Fig. 4 in number percentage (*N*%). PSDs are continuous. However, the main peak of the distribution is shown to vary from sample to sample, even within the same milling technique. Such an observation remarks the need to always provide the PSD of powders used in agronomic pot tests. Standard Samples are all relatively homogeneous whereas over milling results in significantly different behavior of certain samples with respect to their equivalent Standard Samples. In the 150OM set, ARD21 and MCA11 exhibit a bimodal distribution, with two distinct peaks. ARD21, ARD22, MCA11, MCA23 and MCA41 are very responsive to the 150OM milling procedure, meaning that the generation of very small particles is enhanced with respect to the other samples, and is confirmed by the increase in BET-SSA (Fig. 5b). Based on PSD data, these samples also show larger particles if milled according to the 45OM procedure (Fig. 4c), suggesting electrostatic agglomeration of a large number of smaller particles. In 45OM samples, bimodal populations are more pronounced, again suggesting agglomeration of finer particles because of prolonged comminution (Supplementary Table S2). HPGR samples are all very homogeneous, with the exception of syenites from the MCA intrusions (MCA11, MCA12, MCA23, MCA41), which PSD shows a markedly high number of small particles, as confirmed by data reported later in Table 5. Note that the PSD based on

Table 5
Number percentage (*N*%) of fines (particles <0.5 μm) for all powder samples. Samples are ordered by increasing *N*% in Standard Samples.

	Standard Samples	150OM	45OM	HPGR
EBT10 (F)	52.8	58.5	92.0	39.9
MCA11 (C)	58.0	93.6	85.0	99.6
EBT09 (M)	60.5	48.6	93.1	45.6
ARD05 (C)	61.0	46.9	93.1	40.4
ARD22 (M)	61.8	98.7	84.3	46.8
MCA41 (M)	63.5	95.3	83.4	57.7
MCA12 (F)	63.8	46.5	91.3	99.6
EBT13 (M)	64.2	46.5	92.2	40.3
EBT12 (M)	65.9	56.2	88.1	43.0
ARD21 (M)	66.5	82.1	82.4	40.4
MCA23 (M)	77.7	95.4	84.8	99.6
MCA04 (M)	80.1	67.4	91.2	41.5
Average	65 ± 8	70 ± 22	88 ± 4	58 ± 26

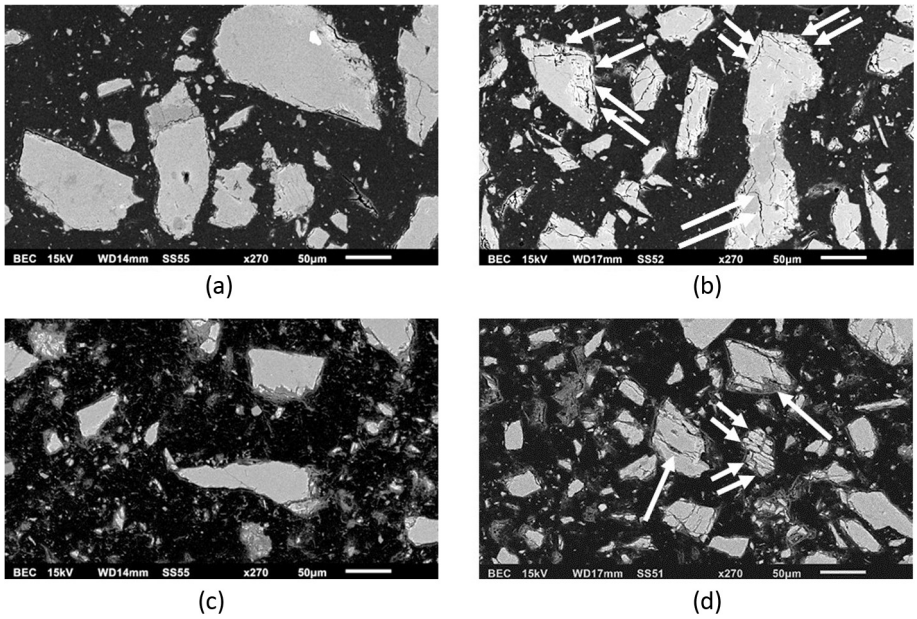

Fig. 6. SEM back-scattering images of selected samples: (a) MCA12 Standard Sample (b) MCA11 Standard Sample (c) MCA12 HPGR sample and (d) MCA11 HPGR sample. SEM imaging demonstrates that MCA12 particles are relatively pristine, whereas MCA11 tends to fracture and crack, especially under the effect of HPGR grinding. White arrows point at areas where cracking is particularly evident.

volume percentage (*V*%) given in Supplementary Fig. S5 reveals the presence of larger particles, as confirmed by visual observation of the powders (Fig. 6).

Here, we define *fines* all those particles arbitrarily chosen to be <0.5 μm. The fines number percentages as a function of the comminution technique are shown in Table 5. For the same sample, different comminution procedures lead to a different amount of fines. Fast dissolving small particles have been invoked to explain the initial leaching rate of K^+ ions from K-feldspar (White and Brantley, 1995). It has been demonstrated that for larger K-feldspar particles leaching is directly proportional to SSA; for particles between 300 μm and 38 μm leaching is independent on SSA; for smaller particles (<0.1 μm) assessment of the leaching rate is expected to increase exponentially with increasing SSA, but is difficult to determine accurately (Holdren and Speyer, 1985). There is no correlation between the granulometry in thin sections (i.e., d_A) and the number of fines in the powder. Likely, the petrographic characteristics of the syenites determine some of the mechanical properties that affect comminution, but fine grains in thin sections are not enough to justify an enhancement in the content of fines in the powder samples. However, fine-grained samples typically required the smaller amount of energy for grinding (Supplementary Table S2). As expected, increasing milling time (i.e., Standard Samples → 150OM → 45OM) increases the number of fines on average. Comminution by HPRG is suggested as a better option for industrial handling of agromineral fertilizers since it leads to a similar to higher amount of fines and higher surface areas than ball milling, for comparable or lesser energy consumption (Supplementary Table S2). In ball mills, fine-grained syenites are preferred.

3.2.3. Surface area: G-SSA and BET-SSA

G-SSA and BET-SSA values are given in Fig. 5(a) and (b), respectively. Values are higher than previously reported (Table 1), although here we work with unrefined raw materials (ultrapotassic syenite) rather than pure minerals (K-feldspar). It is shown that within each comminution technique the G-SSA values are similar for all samples, except for the 150OM samples belonging to the EBT intrusion, in agreement with the PSD results. BET-SSA values (Fig. 5(b)) take into account complex surface features, since they are determined by the adsorption of Kr atoms at the surface of the material and, as such, they are sensitive to roughness at the nanometer scale. Therefore, a distinct grouping of samples cannot be made. 150OM samples and 45OM samples exhibit a BET-SSA that is on average 1.3 times and 2.2 times, higher than Standard Samples, respectively. HPGR samples show similar BET-SSA to those of 150OM samples, most likely due to formation of cracks (Section 3.2.3). This confirms better grinding performance of the HPGR than the ball mill. Each syenite responded differently to the chosen milling technique.

Perhaps, mineralogical composition could explain such a behavior. However, as shown in Supplementary Text S3, there seems to be only a very weak correlation between microcline, the major component of the syenite, and the BET-SSA. Correlations to other minerals could not be identified. Further studies are necessary to ascertain the relationship between mineral content, physical properties (e.g., density and hardness) and response to comminution. Prolonged over milling (45OM) results in more homogeneous values of BET-SSA across the entire set of samples. Overall, our results show that although specific samples exhibit specific characteristics, comminution and sieving can be operated intentionally in order for all the powders to exhibit similar properties.

3.2.4. Imaging of powder particles

To evaluate better the response of the raw materials to comminution, we imaged the powder particles of all samples. Meticulous observation of such particles provides information on cracking and fracturing. Example SEM backscattered electron images of MCA11 and MCA12 for both Standard Samples and HPGR samples are given in Fig. 6. Additional selected images are given in Supplementary Fig. S7. It is shown that with both comminution techniques particles of MCA11 are fractured, whereas MCA12 exhibits relatively pristine grains (Fig. 6). This difference in fracturing behavior can explain, at least partially, the higher BET-SSA observed for MCA11, a medium-to-coarse sample (Fig. 5b). Overall, HPGR enhances fracturing (Supplementary Fig. S7) so that on average the BET-SSA values for HPGR samples are similar to those of

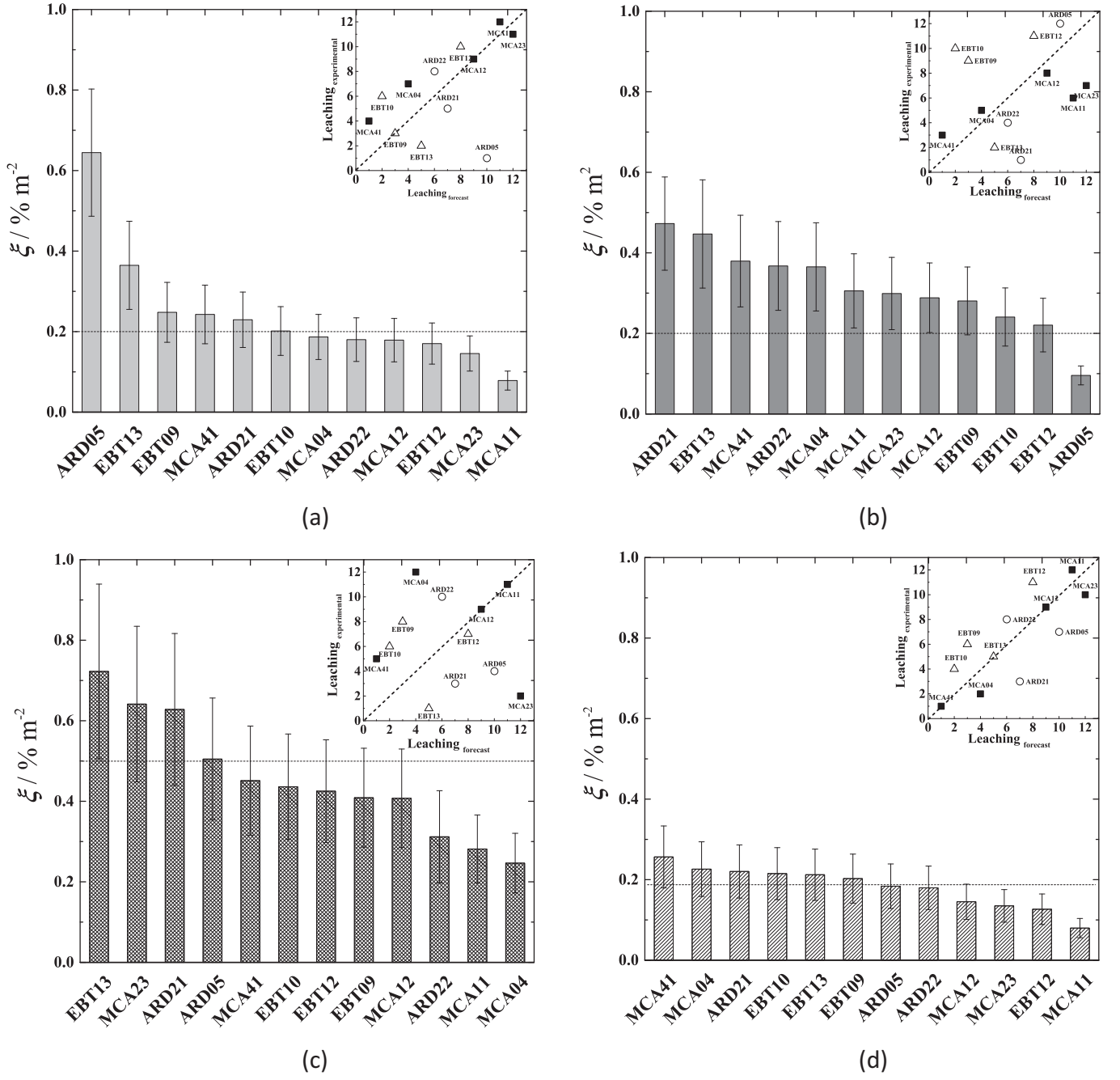

Fig. 7. Potassium extraction efficiency (ξ) for (a) Standard Samples (b) 150OM, (c) 45OM and (d) HPGR samples. Leaching conditions: pH = 1 (HNO_3), 24 h, solid-to-liquid ratio 1:10. Error bars are determined according to Eq. (2). Parity plot ($y = x$ for reference) provided exclusively to aid the comparison between rankings of samples according to experimental leaching and the forecast provided in Table 2. Dashed horizontal line is the average value. ξ values are normalized by BET-SSA (Eq. (1)).

150OM samples, and ~ 30% higher than for Standard Samples. Finer-grained samples such as MCA12 seem to be less susceptible to cracking.

3.2.5. K^+ leaching

The K extraction efficiency (ξ) as defined in Eq. (1) is given in Fig. 7 for all sets of powders. Extraction efficiencies for additional key elements (Si, Al, Ca, Mg, Na, Fe) are given in Supplementary Text S4. Although leaching tests were performed in a strongly acidic solution that might not be representative of soil conditions, our approach is justified because such conditions permit a better discrimination of those subtle differences in leaching behavior exhibited by each of the samples. For all samples, extraction efficiency was <1%. Here, we do not delve in assessing if such an extraction can provide an absolute amount of potassium that is sufficient to fertilize crops in field conditions. Rather, we aim to propose a rationale for selecting the most promising materials that agronomists should test in those field conditions. Manning has demonstrated that syenitic K-feldspar can indeed act as a source of potassium available for plant growth (Manning et al., 2017).

On average, the extraction efficiency was 0.2% m^{-2} for both Standard Samples and HPGR samples, 0.3% m^{-2} for 150OM samples and 0.5% m^{-2} for 45OM samples. Therefore, on average, over milling improves the extraction per unit area, which is a particularly important factor to consider during scale up to industrial production of pulverized agrominerals. The majority of samples are

shown to have a comparable K^+ leaching rate under the experimental conditions used in this study. However, there are significant variations in end-member samples, with MCA41 and MCA11 consistently ranked as one of the fastest and slowest K^+ releaser, respectively. This observation confirms our hypothesis that "feldspar" is a too broad category for agronomic classifications of agrominerals. Therefore, while at the length scale of mining (meters) relevant characteristics are the average parameters of agrominerals (e.g., K_2O content), at the length scale of crop roots (μm), different agrominerals can exhibit different leaching behavior, due to geochemical and mineralogical differences in the intrusion of origin. Such differences can be further accentuated when the microfluidic nature of mineral dissolution in soils is taken into account (Ciceri and Allanore, 2015). Powder features might have important implications for industrial scale handling of agrominerals, but they do not necessarily have a major impact on leaching. However, a sample-dependent, nonlinear increase of the total surface area as a function of comminution (Fig. 4) can be exploited to modulate the total amount of potassium leached as a function of agricultural needs in the field.

In Table 2, a ranking of the K^+ leaching was forecast based solely on petrographic information. In the MCA intrusion sample MCA41 presents Kfeldspar with low degree of AlSi ordering, with medium to fine anhedral crystals, strongly fractured and with intense alteration, all characteristics that in our hypothesis favor K^+ leaching. Conversely, MCA11 and MCA23 exhibit characteristics of a crystallization that occurred under a slow cooling rate, which produced highly ordered, medium-to-coarse and subhedral-to-euhedral crystals, which are poorly fractured, and with minor alteration. These are all characteristics that in our hypothesis disfavor leaching. The proposed leaching ranking for this intrusion was MCA41 > MCA04 > MCA12 > MCA11 > MCA23, which, other than for the last two samples, is confirmed experimentally for both Standard Samples and HPGR milling (Fig. 7a and d insets). Petrography can provide only bulk related properties, suggesting that for outlier samples such as MCA23 some surface parameters (e.g., defects) or particles properties (e.g., fines) are determinging the leaching of potassium. This is further discussed later in Section 3.3.

In the EBT intrusion, fine-to-medium and subhedral K-feldspar crystals in EBT10 and anhedral crystals in EBT09 (Table 2), suggest a faster K^+ leaching rate for these two samples. Furthermore, K-feldspar is moderately-to-strongly fractured, and present a major alteration in both samples. Slower K^+ leaching would be expected from EBT12, which shows medium-to-coarse and subhedral-to-euhedral K-feldspar, typical of grains with high degree of Al-Si ordering. Additionally, the crystals are well-preserved, and only slightly fractured. An overall leaching ranking EBT10 > EBT09 > EBT13 > EBT12 was proposed, which is partially confirmed for both Standard Samples and HPGR powders (inset Fig. 7a and d). However, the extraction efficiency were very similar for all samples, making the overall ranking less valuable.

Lastly, for the ARD intrusion, the three samples (ARD21, ARD22, and ARD05) show very similar petrographic characteristics, which suggest very similar K^+ leaching and an uncertain forecast. An overall leaching ranking ARD22 > ARD21 > ARD05 was proposed, which is not confirmed by experimental data. For the ARD intrusion, only HPGR samples show very similar leaching (inset Fig. 7d), meaning that the petrographic description is able to capture with relative precision the chemical behavior observed in leaching tests only for HPGR powders. Otherwise, the effect of ball comminution seems to erase the conclusions based on petrography. ARD05 shows a particularly high leaching when comminuted in a ball mill.

Comminution of agromineral samples might introduce key features for nutrient leaching such as (i) (surface) defects (ii) fines (iii) preferred particle morphologies (iv) other mechanical effects (e.g., cracking and fracturing). A detailed study of defects was not performed here. However, it is noted that for Standard Samples the petrographic forecast of the leaching is in good agreement with the experiment. Instead, by moving towards over milling procedure in a ball mill, the relationship between petrography and leaching is progressively lost (compare insets in Fig. 7). Petrographic features are important, but cannot be the exclusive variables determining the leaching, since thin-section samples provide limited information on the actual surface reactivity of powders. Over the short term, the main site of potassium leaching is the surface rather than the bulk (Ciceri and Allanore, 2015). In summary, experimental data indicate that in absence of extensive defect structures caused by comminution (i.e., over milling), petrographic features are a good indicator of potassium leaching. Along the series Standard Samples → 150OM → 45OM it is likely that those complex defect structures are progressively generated at the surface. HPGR comminution occurs very quickly (Supplementary Table S2), generating minimum amount of defects, so that similarly to Standard Samples, petrographic considerations suffice to forecast the leaching. Leaching results also suggest that blends of different syenitic rocks comminuted according to different techniques can be used to supply nutrients at different rates thus modulating their supply as a function of the crop actual requirement.

Lastly, note that the data presented in Fig. 6 are normalized by BET-SSA, implying that leaching occurs from a surface which elemental content is homogeneously distributed, and with the surface area being the same as the reactive surface area. Although such assumptions are likely to hold true for major elements such as K, Al and Si, they do not necessarily apply to accessory elements of the syenites, for example Na. Albite and aegirine are the only Na-bearing phases. Albite is largely perthitic, meaning that is not necessarily contributing to the surface of the powder, and questioning BET-SSA normalization. The leaching tests for Na (Supplementary Fig. S12) show that the extraction efficiency decreases systematically with increasing surface area of ball milled samples (i.e., Standard Samples → 150OM → 45OM), suggesting that the value of BET-SSA cannot be associated to particular phases anymore, albite and/or aegirine in this case. However, comparison across set of samples comminuted in the same way remains meaningful with this approach. Note also that comminution might affect the mineralogy of the sample (Fig. 3).

3.3. Correlation between syenite properties and K^+ leaching

In the present study, twelve syenite samples obtained from three cogenetic intrusions have been shown to exhibit distinct petrographic features, similar powder properties but again distinct leaching behavior. To better visualize the correlation between key parameters and reduce the number of variables to describe the set of agrominerals, we performed a Principal Component Analysis (PCA) (Jolliffe, 2002). The following variables were chosen as input of the PCA:

- **parameters related to geology**: (i) K_2O content (Table 4) (ii) area-averaged grain size in thin section d_A (Fig. 2).[1] Intrusions are identifiable by the first three letters in the sample name.
- **parameters related to comminution**: (iv) number of fines (Table 5), (v) energy consumption (Supplementary Table S2)
- **parameters related to leaching**: extraction efficiency (Fig. 7)

Note that PCA was performed on measurable quantities only, and does not include petrographic observations (e.g., extent of alteration) which are difficult to quantify numerically. XRPD data

[1] The shape-related parameter (AR) was ignored as it was approximately 2 in all samples (Supplementary Text S1).

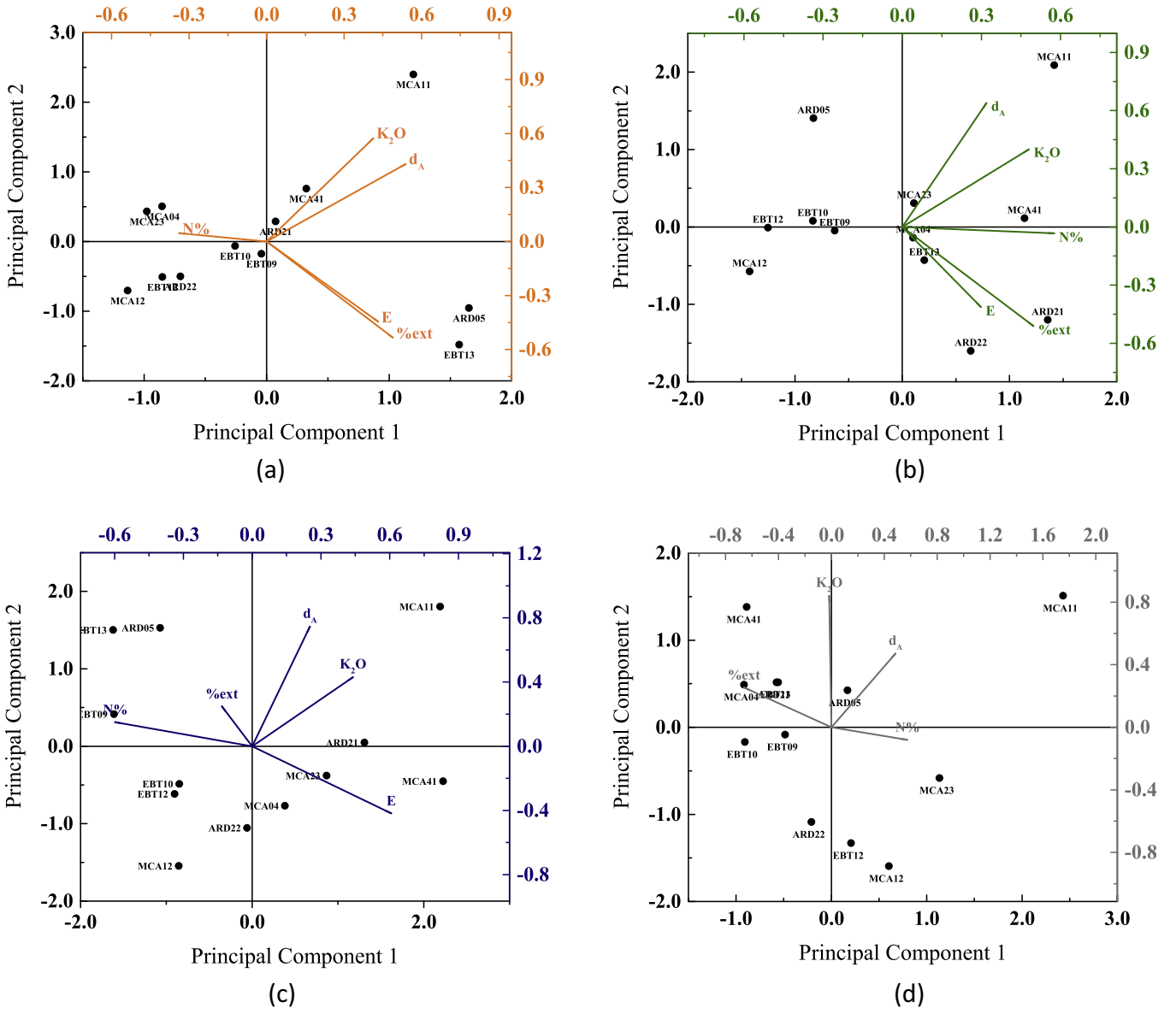

Fig. 8. Loading-scoring biplot for Principal Component Analysis (PCA) on selected properties of syenites. Variables have negative correlation if they are shown on opposite sides. Samples are dominated by the same variables if they lie on the same side. (a) Standard Samples (b) 150OM samples (c) 45OM samples (d) HPGR samples (milling energy not included since it was assumed to be the same for all samples as shown in Supplementary Table S2). Loading of the components read on the top *x* axis and right *y* axis. Scoring of samples read on the bottom *x* axis and left *y* axis. %ext corresponds to ξ.

were excluded as they are directly correlated with the elemental content (i.e., K_2O wt% $\propto$ K-feldspar wt%) and would act as confounding variables. Accessory and varietal minerals were considered irrelevant to potassium leaching. Scoring-loading biplots of the principal components analyses are given in Fig. 8. Correlation matrices are given in Supplementary Table S5.

For Standard Samples (Fig. 8a), PCA shows that the variable most closely correlated with the potassium leaching is the energy input used during milling. Fines, that on surface energy considerations would be presumed to give a major contribution to leaching, are instead shown to be anticorrelated to it. However, in this study, the chemical and mineralogical composition of the fines was not determined. It is possible that non-perthitic albite and other accessory minerals break down into smaller particles during comminution, resulting in a distinct chemical composition of the fines. Overall, samples with the highest K^+ leaching rate are those that received the highest energy input during milling, which in turn was necessitated by the larger grains in the original texture. Samples with the highest number of fines are those with the higher K_2O content, but neither the fines nor the grade results in the highest leaching rates. Most likely, a larger energy input results in an excess of defects and surface energy, which both act to enhance the leaching rate. A logic sequence is then the following: *larger grains → more energy during milling → more defects → higher leaching rate (fines do not matter).*

For the 150OM set (Fig. 8b), leaching is still dependent from the total energy input, but seems to become more influenced by the content of fines. Fines are most likely the results of the mechanical properties of the rocks, and can therefore be ascribed to the intrusion of origin and the K_2O (or K-feldspar) content, as confirmed in Fig. 8b. A logic sequence is then the following: *larger grains in bulk samples are not important due to over milling → similar defects concentration throughout all samples due to over milling → leaching rates more dependent on fines rather than defects.*

For 45OM samples no immediate grouping or specific features can be pointed out, although we note that the fines rather than

the energy input determine the extraction percentage. The amount of fines become uncorrelated to d_A, consistently with an exacerbating over milling procedure. The leaching behavior is not easily resolvable, confirming that an excessive energy input during milling lead to nonlinear changes in physicochemical characteristics of the material, and amorphization of the same, as confirmed by XRPD (Fig. 3).

Finally, given the short milling time and energy input consistent for all samples, HPGR powders could be considered as the best proxy of "ideal samples", where comminution artefacts are minimized. Note that in this case the leaching is very similar for all samples (Fig. 7d). In Fig. 8d, it is shown that K_2O content and d_A are the variables that highly correlate with the potassium extraction percentage, which is consistent with the hypothesis that the behavior of HPGR samples is mostly determined by petrographic characteristics.

Overall, our study reveal a complex interplay of variables related to geological history, comminution, and leaching behavior of samples. Only a comprehensive approach to such an interplay can make agrominerals a valid and successful alternative to soluble potash. It is worth nothing that the K_2O grade that one would intuitively assume as the most important property of the raw material, does not necessarily relate directly to the potassium leaching of a specific sample, although it might influence the mechanical properties during comminution. The relationship between the leaching of potassium and that of other nutrients is discussed in Supplementary Text S5.

4. Conclusion

Agrominerals are relatively high-grade, abundant, and accessible resources with potential for large-scale deployment as fertilizers alternative to soluble salts. Their potential needs to be fully vetted and better elucidated, especially in resource-limited settings facing immediate depletion of soil nutrients. Detailed understanding of the relationship between structure (i.e., geological characteristics) and property (i.e., leaching kinetics) is necessary, and it can be accomplished only through a holistic understanding of petrographic, mineralogical and chemical behavior of both bulk and powder samples.

Here, we have characterized a set of twelve Brazilian ultrapotassic syenites from three different intrusions, which are cogenetic, but not comagmatic. The first intrusion (ARD) is more homogeneous than the others are, with more preserved and larger K-feldspar grains, higher Al-Si ordering and lower K^+ leaching. The second (EBT) and third (MCA) intrusion exhibit larger variations in potassium leaching, likely due to magmatic, tardi-magmatic and postmagmatic processes in the syenitic body. Syenites have similar chemical composition and mineralogy, which, however, do not suffice to explain the leaching behavior at short time scale. Either from the same intrusion or not, each syenite has its own crystallization history, that required a sample-by-sample petrographic description of the K-feldspar features. We demonstrate that such a description of textures, degree of alteration and fracturing as well as the relationship between mineral phases are key to forecast the leaching kinetics, unless major defects concentration arises from comminution.

Preparation of agrominerals for pot and/or field tests should consider the following conclusions: (i) a simple and relatively inexpensive photographic description of thin-section samples can be used to provide an estimation of grain sizes, which correlates with the energy required for milling (ii) the milling energy is most likely the source of defectual structures, which are key for nutrient leaching; if a ball mill is the only option available, samples with the larger grain sizes will most likely require a higher energy input, resulting in increased defects formation and higher potassium leaching; if an HPGR is available, then petrographic descriptors can be used to rank samples based on their forecast leaching (iii) over milling procedures can be used to increase potassium extraction, but the leaching forecast becomes uncorrelated to petrographic considerations (iv) a detailed description of the actual agromineral used in agronomic tests should always be given since "K-feldspar" is a too generic term (v) coupling of comminution with blends of different agrominerals can be engineered to supply different nutrients at different rates.

We envisage important consequences of our findings in agronomy, for which we establish a rationale to guide selection and comminution of agrominerals. However, all those sectors where K-feldspar is a key raw material, for example the ceramic and glass industries, will benefit from this research.

Funding sources

This work was supported by Tavarua Invest.

Appendix A. Supplementary material

Supplementary data associated with this article can be found, in the online version, at http://dx.doi.org/10.1016/j.mineng.2016.11.016.

References

Abdel-Mouty, M.M., El-Greadly, N.H., 2008. The productivity of two okra cultivars as affected by gibberilic acid, organic N, rock phosphate and feldspar applications. J. Appl. Sci. Res. 4, 627–636.
Allen, T., 1997. Particle Size Measurement. Surface Area and Pore Size Determination, 5th ed., vol. 2. Chapman and Hall.
Badr, M., 2006. Efficiency of K-feldspar combined with organic materials and silicate dissolving bacteria on tomato yield. J. Appl. Sci. Res. 2, 1191–1198.
Bakken, A.K., Gautneb, H., Myhr, K., 1997. The potential of crushed rocks and mine tailings as slow-releasing K fertilizers assessed by intensive cropping with Italian ryegrass in different soil types. Nutr. Cycl. Agroecosyst. 47, 41–48.
Bakken, A., Gautneb, H., Sveistrup, T., Myhr, K., 2000. Crushed rocks and mine tailings applied as K fertilizers on grassland. Nutr. Cycl. Agroecosyst. 56, 53–57.
Baligar, V., Fageria, N., He, Z., 2001. Nutrient use efficiency in plants. Commun. Soil Sci. Plant Anal. 32, 921–950.
Berner, R.A., Berner, E.K., 1997. In: Tectonic Uplift and Climate Change. Springer, pp. 353–365.
Blum, A.E., 1994. In: Parsons, Ian (Ed.), Feldspars and their Reactions, vol. 421. Kluwer Academic Publishers.
Bolland, M., Baker, M., 2000. Powdered granite is not an effective fertilizer for clover and wheat in sandy soils from Western Australia. Nutr. Cycl. Agroecosyst. 56, 59–68.
Brown, W.L., Parsons, I., 1984. The nature of potassium feldspar, exsolution microtextures and development of dislocations as a function of composition in perthitic alkali feldspars. Contrib. Miner. Petrol. 86, 335–341.
Brunauer, S., Emmett, P.H., Teller, E., 1938. Adsorption of gases in multimolecular layers. J. Am. Chem. Soc. 60, 309–319.
Ciceri, D., Allanore, A., 2015. Microfluidic leaching of soil minerals: release of K+ from K Feldspar. PLoS ONE 10, e0139979.
Ciceri, D., Manning, D.A., Allanore, A., 2015. Historical and technical developements of potassium resources. Sci. Total Environ. 502, 590–601.
Coroneos, C., Hinsinger, P., Gilkes, R., 1996. Granite powder as a source of potassium for plants: a glasshouse bioassay comparing two pasture species. Fertilizer Res. 45, 143–152.
FAOSTAT database. (Food and Agriculture Organization of the United Nations).
Ferreira, V., Sial, A., 1986. The peralkalic magmatism in the Precambrian Cachoeirinha-Salgueiro foldbelt, Northeast Brazil: geochemical aspects. Revista Brasileira de Geociências 16, 73–85.
Flude, S., Lee, M.R., Sherlock, S.C., Kelley, S.P., 2012. Cryptic microtextures and geological histories of K-rich alkali feldspars revealed by charge contrast imaging. Contrib. Miner. Petrol. 163, 983–994.
Foley, J.A. et al., 2011. Solutions for a cultivated planet. Nature 478, 337–342.
Gautneb, H., Bakken, A.K., 1995. Crushed rocks, minerals and mine tailings as sources of potassium in agriculture. Nor. Geol. Unders. 427, 119–122.
Han, H.S., Jung, J.S., Lee, K.D., 2006. Rock phosphate-potassium and rock-solubilising bacteria as alternative, sustainable fertilisers. Agron. Sustain. Dev. 26, 233–240.
Hang, P.T., Brindley, G., 1970. Methylene blue absorption by clay minerals. Determination of surface areas and cation exchange capacities (clay-organic studies XVIII). Clays Clay Miner. 18, 203–212.

Harley, A., Gilkes, R., 2000. Factors influencing the release of plant nutrient elements from silicate rock powders: a geochemical overview. Nutr. Cycl. Agroecosyst. 56, 11–36.
Hartmann, J. et al., 2013. Enhanced chemical weathering as a geoengineering strategy to reduce atmospheric carbon dioxide, supply nutrients, and mitigate ocean acidification. Rev. Geophys. 51, 113–149.
Hellmann, R. et al., 2012. Unifying natural and laboratory chemical weathering with interfacial dissolution–reprecipitation: a study based on the nanometer-scale chemistry of fluid–silicate interfaces. Chem. Geol. 294, 203–216.
Hinsinger, P., Bolland, M., Gilkes, R., 1996. Silicate rock powder: effect on selected chemical properties of a range of soils from Western Australia and on plant growth as assessed in a glasshouse experiment. Fertilizer Res. 45, 69–79.
Hodson, M.E., 2006. Does reactive surface area depend on grain size? Results from pH 3, 25 C far-from-equilibrium flow-through dissolution experiments on anorthite and biotite. Geochim. Cosmochim. Acta 70, 1655–1667.
Holdren Jr, G.R., Speyer, P.M., 1985. Reaction rate-surface area relationships during the early stages of weathering – I. Initial observations. Geochim. Cosmochim. Acta 49, 675–681.
Holdren Jr., G.R., Speyer, P.M., 1987. Reaction rate-surface area relationships during the early stages of weathering. II. Data on eight additional feldspars. Geochim. Cosmochim. Acta 51, 2311–2318.
ImageJ Image Processing and Analysis in Java, <http://rsb.info.nih.gov/ij/>.
Jena, S. et al., 2014. Studies on extraction of potassium values from nepheline syenite. Int. J. Miner. Process. 133, 13–22.
Jolliffe, I., 2002. Principal Component Analysis. Wiley Online Library.
Kawano, M., Tomita, K., 1995. Formation of mica during experimental alteration of K-feldspar. Clays Clay Miner. 43, 397–405.
Khan, S., Mulvaney, R., Ellsworth, T., 2014. The potassium paradox: implications for soil fertility, crop production and human health. Renewable Agric. Food Syst. 29, 3–27.
Kleiv, R., Thornhill, M., 2007. Production of mechanically activated rock flour fertilizer by high intensive ultrafine grinding. Miner. Eng. 20, 334–341.
Lasaga, A.C., Luttge, A., 2001. Variation of crystal dissolution rate based on a dissolution step wave model. Science 291, 2400–2404.
Leonardos, O.H., Theodoro, S.H., Assad, M., 2000. Remineralization for sustainable agriculture: a tropical perspective from a Brazilian viewpoint. Nutr. Cycl. Agroecosyst. 56, 3–9.
Manning, D.A., 2010. Mineral sources of potassium for plant nutrition. A review. Agron. Sustain. Dev. 30, 281–294.
Manning, D.A., Baptista, J., Limon, M.S., Brandt, K., 2017. Testing the ability of plants to access potassium from framework silicate minerals. Sci. Total Environ. 574, 476–481.
Merkus, H.G., 2008. Particle size Measurements. Fundamentals, Practice, Quality. Springer.
Mohammed, S., Brandt, K., Gray, N., White, M., Manning, D., 2014. Comparison of silicate minerals as sources of potassium for plant nutrition in sandy soil. Eur. J. Soil Sci. 65, 653–662.
Pretty, J. et al., 2010. The top 100 questions of importance to the future of global agriculture. Int. J. Agric. Sustain. 8, 219–236.
Priyono, J., Gilkes, R., 2004. Dissolution of milled-silicate rock fertilisers in the soil. Soil Res. 42, 441–448.
Priyono, J., Gilkes, R., 2008. High-energy milling improves the effectiveness of silicate rock fertilizers: a glasshouse assessment. Commun. Soil Sci. Plant Anal. 39, 358–369.
Rigby, D., Cáceres, D., 2001. Organic farming and the sustainability of agricultural systems. Agric. Syst. 68, 21–40.
Sánchez, E.C., Torres, M.E., Diaz, C., Saito, F., 2004. Effects of grinding of the feldspar in the sintering using a planetary ball mill. J. Mater. Process. Technol. 152, 284–290.
Schönert, K., 1988. A first survey of grinding with high-compression roller mills. Int. J. Miner. Process. 22, 401–412.
Scovino, J.S., Rowell, D., 1988. The use of feldspars as potassium fertilizers in the savannah of Colombia. Fertilizer Res. 17, 71–83.
Skoog, D., West, D., Holler, F., Crouch, S., 2013. Fundamentals of Analytical Chemistry. Cengage Learning.
Skorina, T., Allanore, A., 2015. Aqueous alteration of potassium-bearing aluminosilicate minerals: from mechanism to processing. Green Chem. 17, 2123–2136.
Smith, J.V., Brown, W.L., 1988. Feldspar Minerals. Volume 1 Crystal Structures, Physical, Chemical, and Microtextural Properties. Springer-Verlag.
Somerwill, K. et al., 2012. Future Need and Role of Potash in UK Food Production. The Food and Environment Research Agency.
Swanson, S., 1977. Relation of nucleation and crystal-growth rate to the development of granitic textures. Am. Mineral. 62, 966–978.
Tavares, L., 2005. Particle weakening in high-pressure roll grinding. Miner. Eng. 18, 651–657.
Teng, H.H., Fenter, P., Cheng, L., Sturchio, N.C., 2001. Resolving orthoclase dissolution processes with atomic force microscopy and X-ray reflectivity. Geochim. Cosmochim. Acta 65, 3459–3474.
Thompson, R., Fowler, M., 1986. Subduction-related shoshonitic and ultrapotassic magmatism: a study of Siluro-Ordovician syenites from the Scottish Caledonides. Contrib. Miner. Petrol. 94, 507–522.
Tilman, D., Balzer, C., Hill, J., Befort, B.L., 2011. Global food demand and the sustainable intensification of agriculture. Proc. Natl. Acad. Sci. 108, 20260–20264.
Tollefson, J., 2010. The global farm. Nature 466, 554–556.
Trewavas, A., 2001. Urban myths of organic farming. Nature 410, 409–410.
Van Straaten, P., 2002. Rocks for Crops: Agrominerals of sub-Saharan Africa. Icraf Nairobi.
Van Straaten, P., 2006. Farming with rocks and minerals: challenges and opportunities. Anais da Academia Brasileira de Ciências 78, 731–747.
Vogel, L., Peukert, W., 2003. Breakage behaviour of different materials—construction of a master curve for the breakage probability. Powder Technol. 129, 101–110.
Von Wilpert, K., Lukes, M., 2003. Ecochemical effects of phonolite rock powder, dolomite and potassium sulfate in a spruce stand on an acidified glacial loam. Nutr. Cycl. Agroecosyst. 65, 115–127.
Wang, J., Zhang, F., Cao, Y., Zhang, X., 2000. Effect of plant types on release of mineral potassium from gneiss. Nutr. Cycl. Agroecosyst. 56, 37–44.
Weerasuriya, T., Pushpakumara, S., Cooray, P., 1993. Acidulated pegmatitic mica: a promising new multi-nutrient mineral fertilizer. Fertilizer Res. 34, 67–77.
White, A.F., Brantley, S.L., 1995. Chemical Weathering Rates of Silicate Minerals, vol. 31. Mineralogical Society of America.
Wilson, M., 2004. Weathering of the primary rock-forming minerals: processes, products and rates. Clay Miner. 39, 233–266.
World Population Prospects: The 2012 Revision, <http://esa.un.org/unpd/wpp/unpp/panel_population.htm>.